SIMULATION ANALYSIS AND EXPERIMENT OF MAGNETIC POLE SHAPE INFLUENCE ON BETATRON MAGNETIC FIELD

by

Qi LIU [1*], Ren-Bo WANG [1], Jin-Hai LI [2], Hai-Tao WANG [1], Hai-Sheng CHEN [3], and Bin TANG [1]

[1]Engineering Research Center of Nuclear Technology Application, Ministry of Education, East China University of Technology, Nanchang, China
[2]China Institute of Atomic Energy, Beijing, China
[3]Pan-China Detection Technology, Nanchan, China

Scientific paper
https://doi.org/10.2298/NTRP2201001L

Betatrons have the advantages of small size, lightweight, and simple operation. They are widely used in non-destructive testing, cargo, and vehicle safety inspection systems. Magnetic field distribution is an essential parameter of betatrons and has been investigated via experimental methods. Recently, simulations have been performed for the magnetic field distribution generated by different magnetic pole parameters. In this study, the finite element method is employed to simulate the magnetic field distribution. The effects of the different magnetic end face opening angles, pole protrusion sizes, number of central magnetic pads, and magnetic pole bottom width on the magnetic field distribution are simulated. Based on the simulation results, magnetic poles are developed, and the magnetic field distribution is measured by a gauss meter. The relative error of the measured and simulated equilibrium orbit is 2.1 %, and the relative error of the magnetic field decay index is 3.3 %. The magnetic field distribution can satisfy the essential conditions that the magnetic field at equilibrium orbit of the betatron is equal to half of the average magnetic field within equilibrium orbit and the magnetic field decay index is greater than 0 and less than 1. The results show that the finite element simulation method and established model have high reliability and effectively improve the design accuracy of magnetic poles.

Key words: betatron, magnetic field, magnetic pole, finite element

INTRODUCTION

Betatrons are devices used to generate high-energy electron beams and X-rays [1]. Since Kerst [2-4] developed the first betatron in 1940, numerous studies have been conducted on betatrons. Betatrons are widely used in non-destructive testing, cargo, and vehicle security inspection systems, and industrial X-ray imaging systems due to their advantages of small size, lightweight, simple operation, no requirement for water cooling, and low cost [5-8].

The core component of a betatron is a magnetic pole (MP) [9]. The MP face shape directly determines the change law of the magnetic field (MF) at the betatron air gap, and electrons are accelerated under the MF at the air gap. An ideal selection of the magnetic end face shape can make the MF produce a stable focusing force on electrons [4] and directly affect the number of electrons captured [10-13] and accelerated as well as the intensity of the bremsstrahlung [14] generated by the betatron. Although many researchers have focused on the parameter improvement of magnetic end faces, the magnetic end face shape is determined using an electrolytic cell model and a gravity model [9], and errors generated using the model test can reach 20-30 %. Using simulation methods, the influence of MP face shape on the corresponding orbit [15] and the MF decay index can be more extensively investigated than using experimental methods.

In this study, the finite element analysis method [16] is employed to establish an MP model of betatron, simulate the spatial distribution of the MF, and optimize the MP shape. The MP were developed based on the simulated data and the MF distribution was measured by a gauss meter. The effects of different magnetic end face parameters on the equilibrium orbit and MF decay index are discussed.

* Corresponding author, e-mail: qil@ecut.edu.cn

METHODOLOGY

Geometric model parameters

The magnet structure of a betatron adopts a Ш-shaped magnetic circuit structure [17]. Figure 1 depicts the cross-section of the magnet structure, which is mainly divided into MP, a horizontal magnetic yoke, a vertical magnetic yoke, and a central magnetic pad. Electrons move under the MF at an air gap between an upper MP (UMP) and a lower MP (LMP). The core of the magnet structure is the MP, and the UMP and LMP face shapes directly determine the MF distribution (MFD) [18-20]. The main parameters of the MP model are as follows: the diameter, the height, the distance between the UMP and LMP, and the diameter of the central magnetic pad, and they are 170 mm, 97 mm, 32 mm, and 70 mm, respectively. The MP, yoke, and central magnetic pad are made of silicon steel sheets.

SIMULATION MODEL

To increase the filling factor of the gap between the UMP and LMP, four central magnetic pads with a thickness of 5 mm were selected in the initial simulation, and the FR4 fibreboard was used for insulation between magnetic pad pairs. The number of turns of the excitation winding [3] was 70 turns, and the number of turns was 8-8-7-6-6 from the inside to the outside. This layout was used to prevent the coil from blocking the X-ray output from the betatron. The simulation geometric model adopts the central 2-D rotational axisymmetric model, which simplifies the geometric structure complexity in the simulation software, and the model conforms to the geometric structure of the actual betatron design. The model simulation calculation uses the electromagnetic

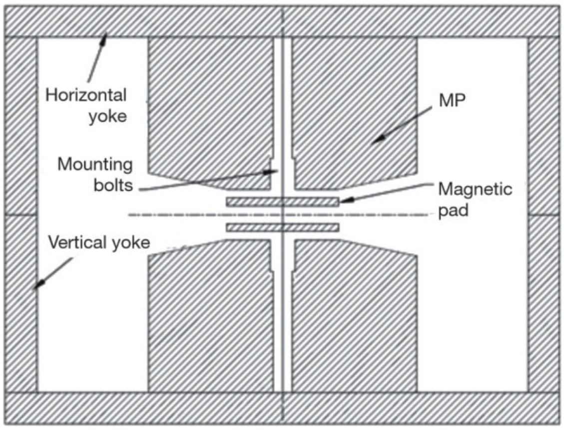

Figure 1. Magnet structure

field physical interface of the alternating current/direct current module of the COMSOL software [21], and the established simulation model is shown in fig. 2.

In fig. 2, the orange, yellow, brown, and light blue domains are the silicon steel sheet, coil, central bolt, air domain, and infinite element domain, respectively. In the simulation calculation, the coil model adopted a single-wire coil group model, and the coil excitation current was 200 A. The mesh sequence type was set to physics control mesh, and the mesh size was set to a finer.

FINITE ELEMENT SIMULATION

Influence of magnetic end face opening angle

The MF used by the betatron is a constant gradient MF. Only by selecting appropriate parameters can the electrons be accelerated in a stable orbit and gener-

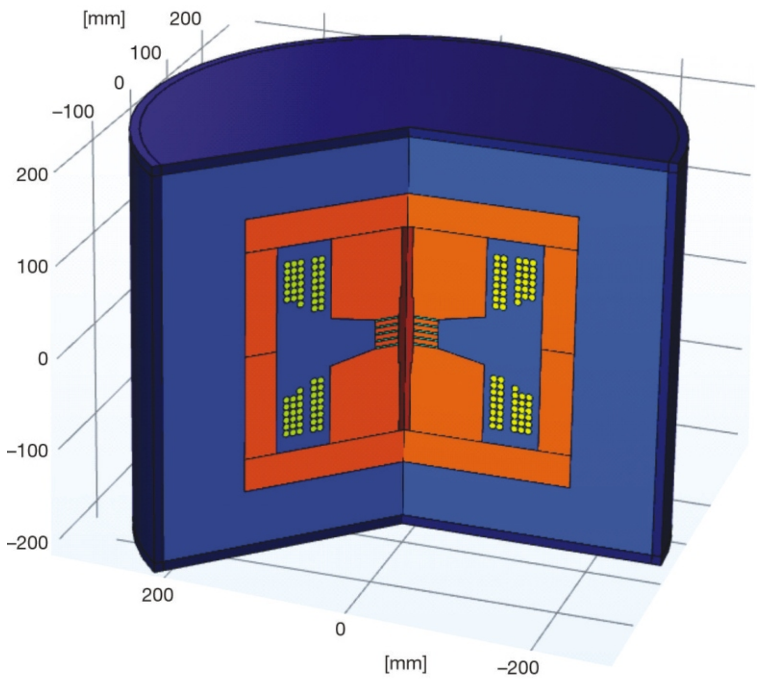

Figure 2. Simulation model

ate a stable focusing force for electrons. The constant gradient MF is rotationally symmetric to the z-axis, and the MF is symmetrical up and down to the central plane of z = 0. Additionally, the change of the axial component of the MF in the air gap between the UMP and LMP with radius r must satisfy the following

$$H_z \quad \frac{C}{r^n} \tag{1}$$

where n is the MF decay index and C is the constant. To make the electrons meet the focusing requirements and avoid resonance due to axial and radial vibrations, the MF decay index should satisfy the condition of $0.5 < n < 1$ [2, 4]. If the MF strength (MFS) on the equilibrium orbit of electron motion is H_0, eq. (1) can be expressed as follows

$$H \quad H_0 \ \frac{r_0}{r}^{\ n} \tag{2}$$

According to the requirement of stable motion of electrons on the equilibrium orbit, the MFS on the electron equilibrium orbit should be equal to half of the average MFS inside the orbit at any time; *i. e.*, the condition of 2:1 [2, 4] must be satisfied, as follows

$$H_0 \quad \frac{\overline{H_0}}{2} \tag{3}$$

The MFD should satisfy eqs. (2) and (3) simultaneously; thus, the MF should only be established within the range of the air gap between the UMP and LMP according to the variation law of eq. (2). To ensure that the MF at the air gap changes according to eq. (2), the two opposite magnetic end faces of the UMP and LMP should have a certain special shape.

Because the magnetic permeability of the MP silicon steel sheet is much larger than that of air, most magnetic resistance of the entire magnet is concentrated in the air gap between the MP, so it can be approximated that the MP surface is equipotential [22]. Thus, we have

$$\lambda_0 H_{0\mathrm{m}} \quad \lambda_x H_{\mathrm{mx}} \tag{4}$$

where λ_x and H_{mx} are the length of the MF lines and MFS in the air gap at the radius r_x, respectively and λ_0 and $H_{0\mathrm{m}}$ are the length of the MF lines and MFS, in the air gap at the equilibrium orbit r_0, respectively. Because the curvature of the MF lines in the air gap between the MP is minute, the length of the MF lines and the air gap between the MP differ by no more than 1-2 %. From eqs. (2) and (4), we have

$$\delta_x \quad \delta_0 \ \frac{r_x}{r_0}^{\ n} \tag{5}$$

where δ_x and δ_0 are the sizes of the air gap between the MP at the radius r_x and equilibrium orbit r_0, respectively. According to the relational expression given by eq. (5), the UMP and LMP faces should be curved surfaces. It is difficult to manufacture a curved surface that conforms to eq. (5) in the actual machining process. However, because the curvature of the curve generatrix is not large, the curved surface can be considered a plane in the simulation calculation, and the angle between the plane and horizontal plane is θ (shown in fig. 3).

The angle θ directly determines the MFD law. According to the geometric model in fig. 3, the MFD along the radial direction of the central plane is calculated when the angle θ is 5°, 10°, 15°, 20°, 25°, and 30° (shown in fig. 4).

From fig. 4, the MFS gradually decreases with an increase in θ, especially in the range of the MP air gap, the decrease is more pronounced. When the angle θ exceeds 20°, the MF falls rapidly at the air gap, changing the MF, which cannot satisfy eq. (3). In the electron acceleration region, the distribution of the average MFS value when θ is 5°, 10°, and 15° is shown in fig. 5.

In fig. 5, the intersection point between the MFS curve and the average curve is the point where the ra-

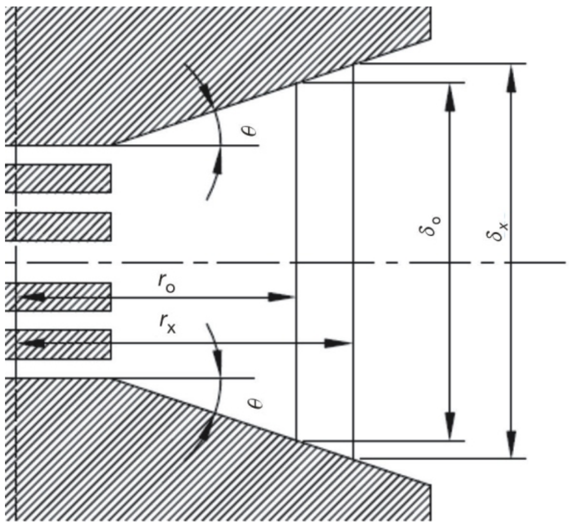

Figure 3. Schematic diagram of MP

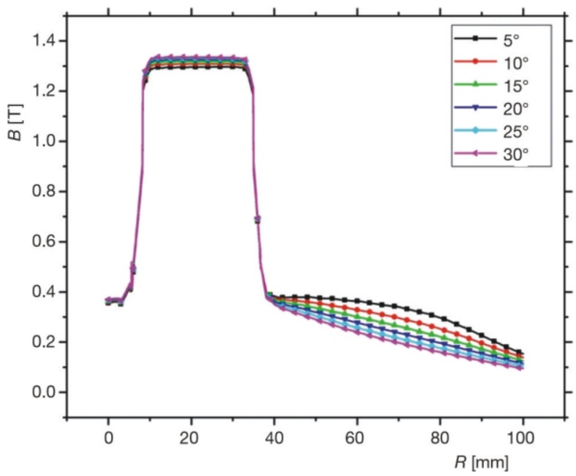

Figure 4. MFD with different opening angles of MP

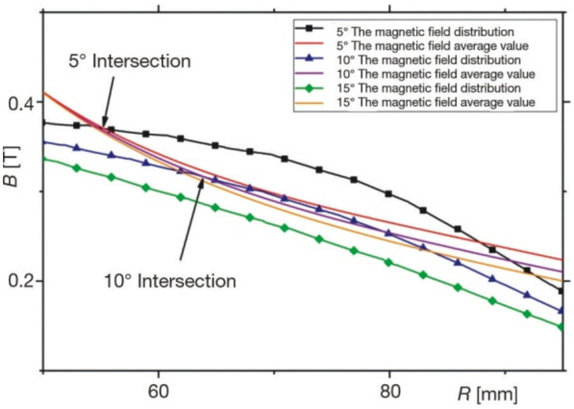

Figure 5. Distribution map of the average value of the MF

dius of the electron equilibrium orbit is located. Clearly, the intersection point only exists when the angle is 5° and 10°, and the two curves have no intersection point when the angle is 15°, which does not satisfy the requirements. The MFD near the equilibrium orbit when the angle is 5° and 10° is shown in fig. 6.

When θ was 5°, the MF decay index n near the equilibrium orbit was 0.331. At this time, $n < 0.5$, which contradicts $0.5 < n < 1$. When θ was 10°, $n = 0.748$, which satisfies $0.5 < n < 1$, so the optimal opening angle of the MP face should be approximately 10°. The distribution of MF lines when θ is 10° is shown in fig. 7.

From fig. 7, the MF lines at the air gap between the MP are bent outward into a barrel shape [15], and the generated MF is a drum-shaped field, which meets the focusing requirements of electrons.

INFLUENCE OF POLE EDGE PROTRUSION

The changing law of MF at the MP air gap must satisfy eq. (2). However, owing to the existence of magnetic flux leakage (MFL) on both sides of the MP edge, the aforementioned law is affected to a certain extent. From fig. 7, some magnetic lines of force penetrate the coil from the edge of the MP to the yoke, and the closer they are to the edge of the MP angle, the more profound they are, causing the MF intensity to fall rapidly near the edge.

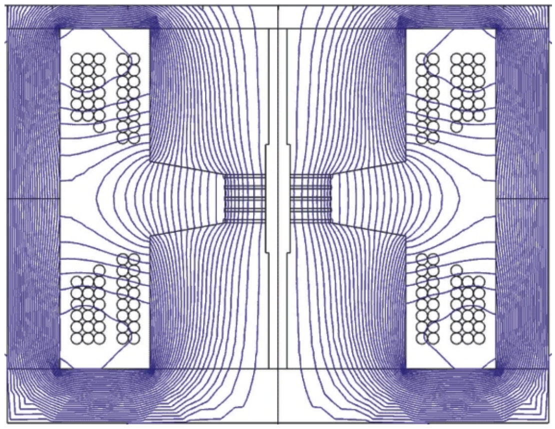

Figure 7. Distribution of MF lines of force with MP opening angle of 10°

To compensate for the MFL at the pole edges, a special protrusion can be used on the pole edges. The structure of the protrusion edge is shown in fig. 8, where h and ω are the height and angle of the protrusion edge, respectively. The MFD with and without protrusion are calculated in COMSOL (shown in fig. 9).

From fig. 9, at the MP edge, the MFS with the protrusion is higher than that without the protrusion, which can effectively compensate for the weakening of the MFS due to the edge MFL. In the actual MP design, there is no special solution method for the protrusion edge size. Generally, the optimal size is selected by testing models with different parameters. The protrusion height is generally between 5 mm and 12 mm. If the protrusion is too high, it will affect the equilibrium orbit. Meanwhile, if the protrusion is too low, the compensation effect is not obvious. The protrusion angle is generally between 20° and 60°. It increases the difficulty of processing silicon steel sheets. In

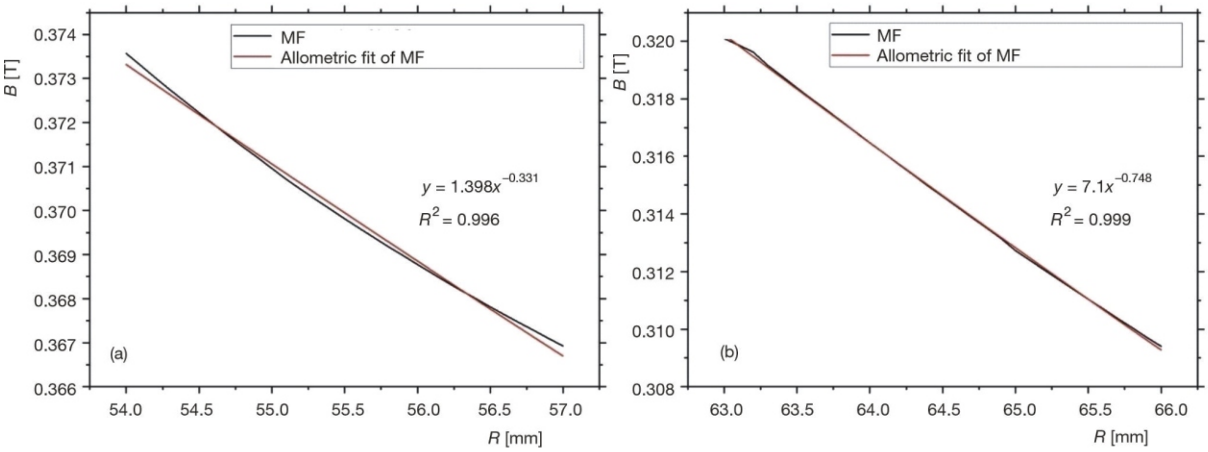

Figure 6. The MFD near the equilibrium orbit: angle: (a) 5°, (b) 10°

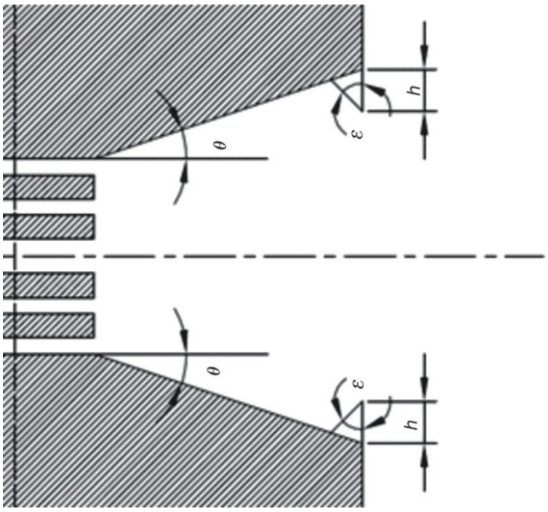

Figure 8. Schematic diagram of the protrusion structure

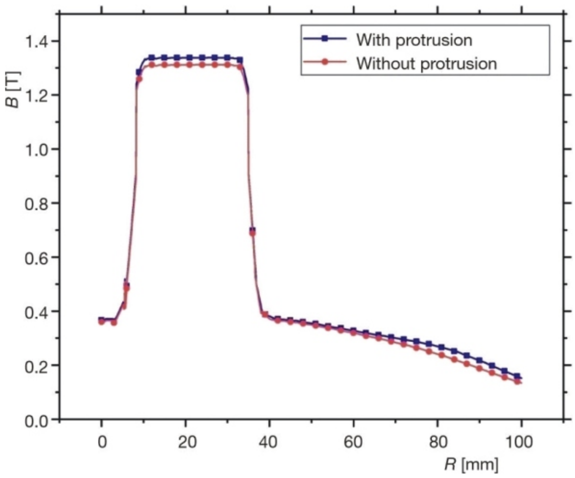

Figure 9. The MFD with and without protrusion

COMSOL, the protrusion edge height is set to 5 mm, and the angle is varied at 20°, 25°, 30°, 35°, 40°, 45°, 50°, 55°, and 60°. The simulation results are shown in fig. 10.

From fig. 10, when the protrusion height is constant, the MFD of different protrusion angles is almost the same, and the protrusion angle insignificantly affects the MFD. Therefore, in the actual design, considering the difficulty and weight of MP processing, the angle can be appropriately selected to be approximately 30°.

The protrusion angle calculated in COMSOL is 30°, and the protrusion heights are 5 mm, 7 mm, 9 mm, and 11 mm. The corresponding MFD is shown in fig. 11. From fig. 11, the higher the protrusion height, the greater the MFS at the MP edge is compensated for. When the height exceeds 9 mm, the MF produces an obvious protrusion, which seriously damages the MF according to eq. (2). Therefore, when designing the protrusion, the height should not exceed 9 mm, it should be approximately 7 mm.

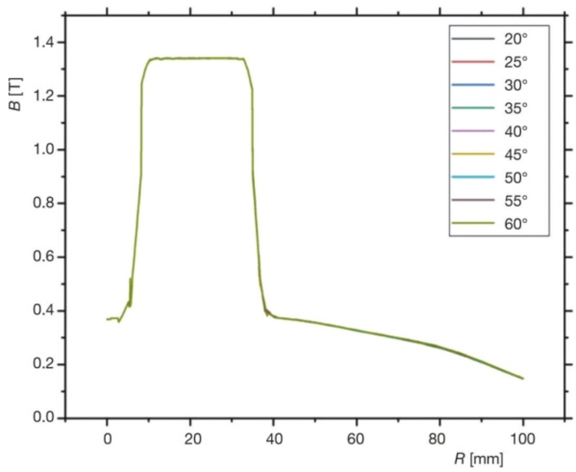

Figure 10. The MFD at different angles when the height of the protrusion is 5 mm

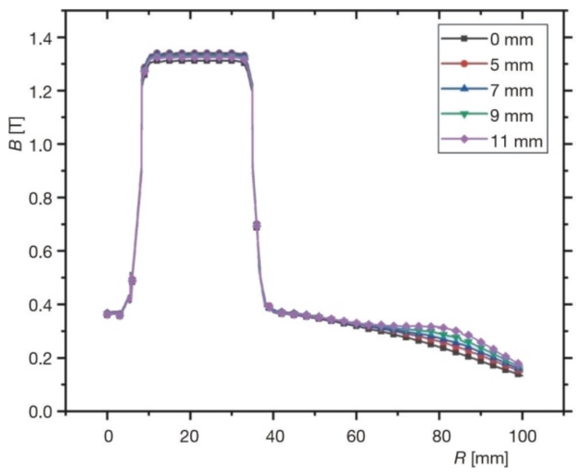

Figure 11. The MFD of different heights when the protrusion angle is 30°

INFLUENCE OF THE NUMBER AND THICKNESS OF THE CENTRAL MAGNETIC PAD

To satisfy the condition of an MF of 2:1, the central magnetic pad with a radius r_c should have the corresponding MFS H_{cm} with the equilibrium orbit. In this part of the inter-pole space, according to eq. (4), the air gap should satisfy the following

$$\delta_c \quad \delta_0 \frac{H_{0m}}{H_{cm}} \tag{6}$$

To adjust the law that the MF in the ring r_0-r_c decays exponentially along the radius, the air gap δ_c should be divided into several small air gaps. For this purpose, a special magnetic pad needs to be placed in the middle of the MP.

A schematic of the structure of placing the central magnetic pad is shown in fig. 12, where $\delta_c = \delta_1 + + \delta_1 + \delta_1$ – the size of the air gap, h_b – the thickness of

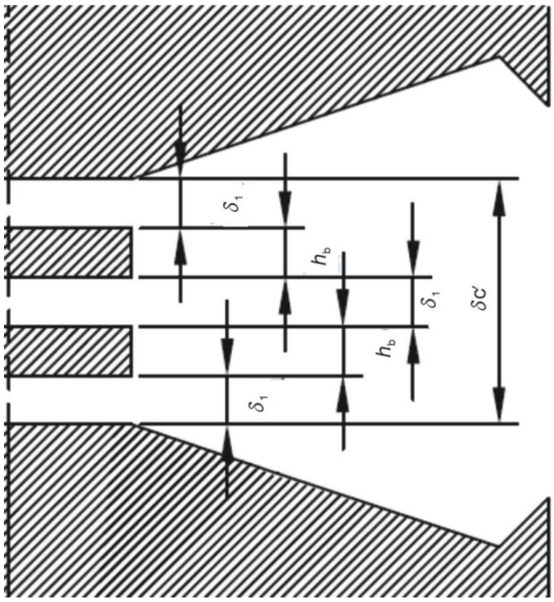

Figure 12. Schematic diagram of the central magnetic pad structure

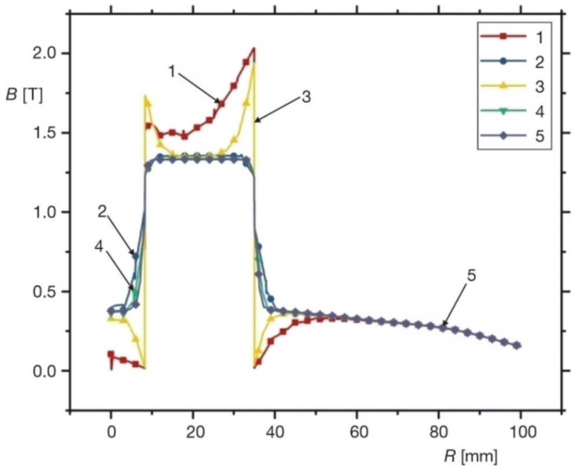

Figure 13. The MFD of different numbers of magnetic pads

the central magnetic pad and δ_c' is the distance between the UMP and LMP at the radius r_c. According to the schematic, the number of magnetic pads can be calculated using the following

$$h_b \quad \frac{\delta_c \quad \delta_c}{m_c} \tag{7}$$

where m_c is the number of magnetic pads. Accordingly, only the requirements of the air gap are considered, and the influence of the magnetic pads on the nearby MF, as well as the equilibrium orbit, is not considered. Further experiments are required to select the optimal number of magnetic pads. When the number of magnetic pads calculated in COMSOL is 2, 3, 4, and 5, the MFD law is shown in fig. 13.

From fig. 13, when one and three magnetic pads are used, the MF lines near the central magnetic pad are severely distorted, and the distorted MF lines cannot meet the electronic focusing requirements, so it is impossible to choose less than three magnetic pads. When four and five magnetic pads are selected, the MFD can well meet the requirements. At this time, the MFD of the electronic equilibrium orbit is shown in fig. 14.

From fig. 14, n = 0.563 and 0.502 for four and five magnetic pads, respectively, both of which meet the MF focusing requirements. The magnetic pad comprises multiple silicon steel sheets stacked and bonded by glue. Considering that the more magnetic pads there are, the thinner the thickness of a single magnetic pad will be, which will significantly increase the processing difficulty of the magnetic pad, choosing four magnetic pads is ideal.

INFLUENCE OF POLE BOTTOM WIDTH

Because the central part of the MP and magnetic pad are much heavier in terms of magnetic flux than the rest of the MP, the MP material cannot be fully em-

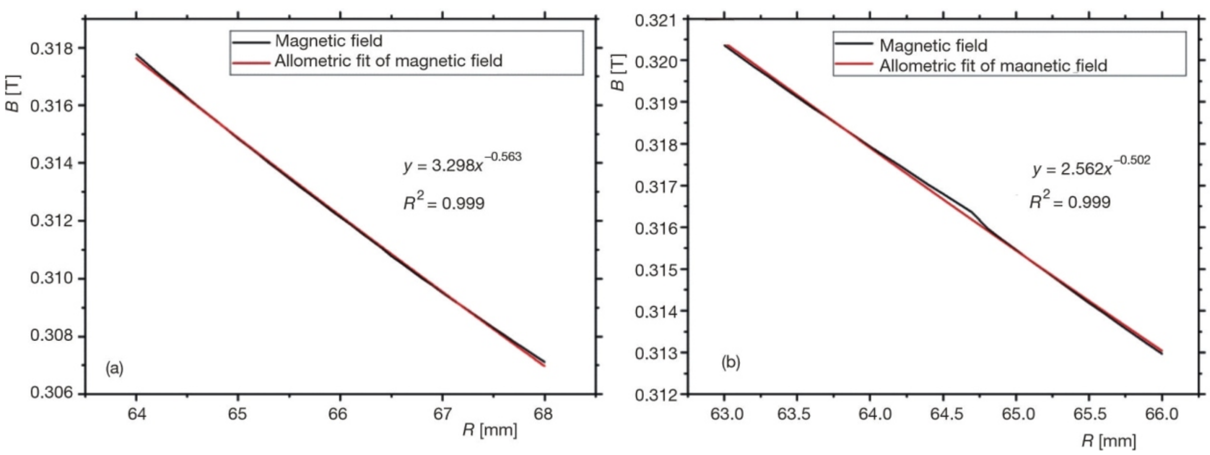

Figure 14. The MFD near the equilibrium orbit: (a) 4 magnetic pads, (b) 5 magnetic pads

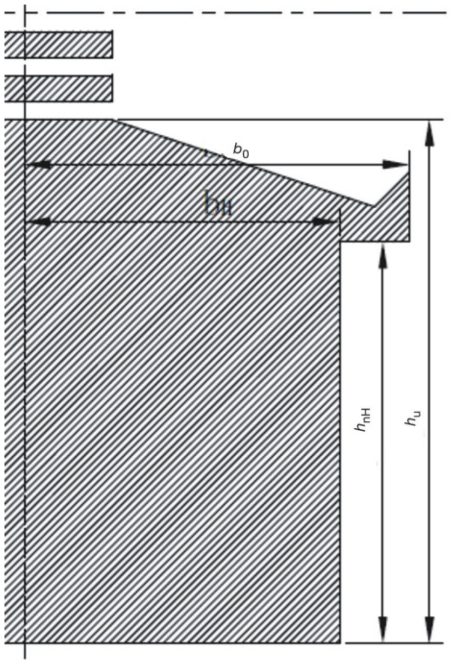

Figure 15. Schematic diagram of optimized magnetic poles

ployed, thereby dramatically reducing the economy of the electromagnet of the entire radiator. To exploit the MP material without destroying the 2:1 and MF focusing conditions, the MP cylinder's bottom width can be appropriately changed (shown in fig. 15).

In the simulation model parameters, b_0 is fixed at 85 mm and the values of b_H are set to 83 mm, 81 mm, 79 mm, 77 mm, 75 mm, 73 mm, 71 mm, 69 mm, 67 mm, and 65 mm in COMSOL. The calculated MFD is shown in fig. 16.

From the fig. 16, as the value of b_H decreases, the MFS at the central magnetic pad decreases gradually, while the change in MFS at the MP air gap is small. This phenomenon will cause a certain deviation from the equilibrium orbit and insignificantly affect the MFD law near the equilibrium orbit.

According to the 2:1 condition, the corresponding equilibrium orbit radius is calculated, and the equilibrium orbit radius is 65.5 mm without reducing the MP cylinder's bottom width, *i. e*., b_H is 85 mm.

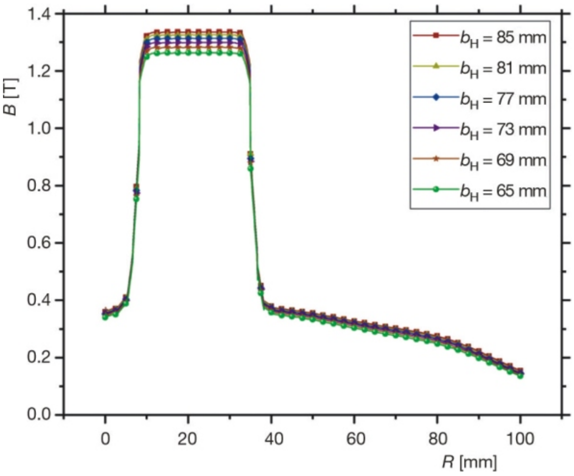

Figure 16. The MFD when b_H is different value

Table 1. Equilibrium orbit radius corresponding to different b_H values

b_H [mm]	Equilibrium orbit [mm]	Error [%]
83	65.5	0
81	65.7	0.3
79	65.9	0.6
77	66.1	0.9
75	66.7	1.8
73	66.7	1.8
71	67.5	3.1
69	67.7	3.4
67	68.4	4.4
65	69	5.3

From tab. 1, when b_H is reduced from 83 to 65 mm, the equilibrium orbit radius gradually increases. When b_H is between 83 and 73 mm, the error of the equilibrium orbit radius can be kept within 3 %, so the MP bottom width can be appropriately reduced. The cylinder radius is approximately 73 mm, which can reduce the MP weight and improve the equipment economy.

EXPERIMENTS AND RESULTS

Based on the results obtained from the previous simulations, we developed the corresponding MP using 0.3 mm silicon steel, as shown in fig. 17.

The parameters of the MP and magnetic pad are shown in tab. 2.

To verify whether the MFD generated by the developed magnetic pole is consistent with the simulation, a magnetic gauss meter is used to test the MFD. The experimental test structure diagram and test system are shown in fig. 18 and fig. 19.

During the test, the excitation power is used to supply power to the excitation windings to generate the necessary excitation current. The Gauss meter probe measures the MFS point by point along the radial direction in the $z = 0$ plane. The MFD test results are shown in fig. 20.

Figure 17. The MP and magnetic pad

Table 2. The MP parameter

Parameter	Value
Height	97 mm
Diameter	170 mm
The MP opening angle	10°
Central air gap height	32 mm
The MP bottom diameter	146 mm
Protrusion height	7 mm
Protrusion angle	30°
Central magnetic pads	4
Central magnetic pad width	70 mm
Central magnetic pad thickness	5.5 mm

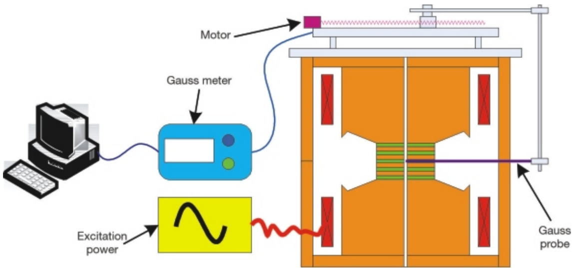

Figure 18. Experimental test structure diagram

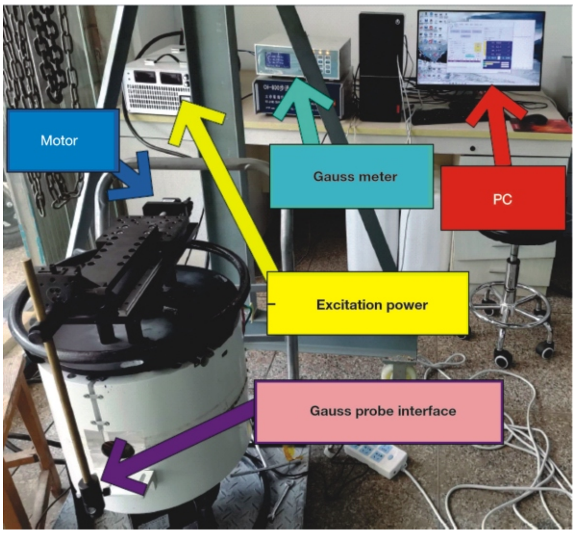

Figure 19. Experimental test system

The measured results are in accordance with the simulated. The MFS decreases slightly in the radial direction inside the central magnetic pad, which may be caused by the unevenness of the silicon steel sheet. In the electron acceleration region, the measured MFS is slightly higher than the simulated value. The parameters near the equilibrium orbit are shown in tab. 3.

The relative error of the equilibrium orbit is 2.1 %, and the relative error of the magnetic field falling index is 3.3 %. Both parameters satisfy the betatron condition. The results show that the values obtained by the finite element software simulation have high accuracy.

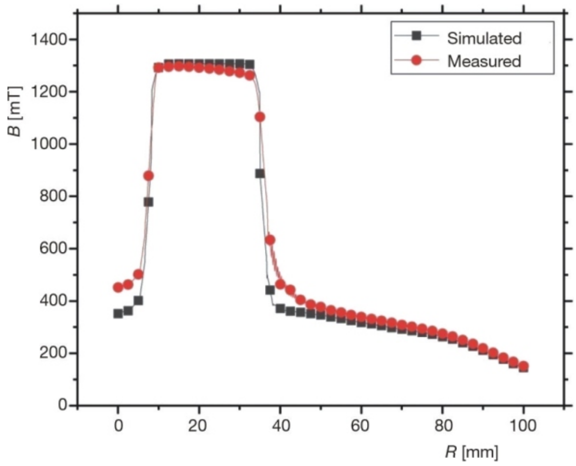

Figure 20. Simulated and measured MFD

Table. 3 Measured and simulated results

Parameter	Measured	Simulated	Relative error
Equilibrium orbit	65.3 mm	66.7 mm	2.1 %
The MF falling index n	0.59	0.61	3.3 %

CONCLUSIONS

In this study, the MF simulation of the betatron based on the COMSOL finite element simulation software is employed, and the MP is developed. The following conclusions are drawn:

The optimal magnetic end face opening angle is 10°.

The MP edge should be designed to be protrusion; the ideal protrusion height and angle are 7 mm and 30°, respectively; the ideal number of central magnetic pads between the UMP and LMP is 4; the MP cylinder's bottom width and radius can be reduced by 12 mm to maintain an equilibrium orbit change within 3 %.

Using an MP of this shape, the radius of the electron equilibrium orbit is calculated as 66.7 mm, and the MF decay index near the equilibrium orbit is 0.61. Based on simulation results, MP is developed and tested. The relative error of the measured and simulated equilibrium orbit is 2.1 %, and the relative error of the magnetic field falling index is 3.3 %. The MFD law satisfies the betatron requirements.

The experimental results prove the accuracy and feasibility of the proposed simulation method. This simulation allows researchers to quickly find the optimal design solution when developing new accelerator models.

ACKNOWLEDGMENT

This work was supported by the National Natural Science Foundation of China (No.12075055), Open Funds of Engineering Research Center of Nuclear Technology Application of the Ministry of Education (No.HJSJYB2020-4).

AUTHORS' CONTRIBUTIONS

Q. Liu: Methodology, Writing original draft. H.-S. Chen: Data curation. H.-T. Wang: Writing – review and editing. J.-H. Li: Supervision. R.-B. Wang: Supervision. B. Tang: Supervision.

REFERENCES

[1] Kerst, D. W., Historical Development of the Betatron, *Nature, 157* (1946), 3978, pp. 90-95
[2] Kerst, D. W., Acceleration of Electrons by Magnetic Induction, *Physical Review, 58* (1940), 9, pp. 841-841
[3] Kerst, D. W., A 20-Million Electron-Volt Betatron or Induction Accelerator, *Review of Scientific Instruments, 1*3 (1942), 9, pp. 387-394
[4] Kerst, D. W., Serber R., Electronic Orbits in the Induction Accelerator, *Physical Review, 60* (1941), 1, pp. 53-58
[5] Chakhlov, S. V., et al., Betatron Application in Mobile and Relocatable Inspection Systems for Freight Transport Control, *Journal of Physics: Conference Series, 671* (2016), 012024
[6] Yu, J.W., Electronic Induction Accelerator for Industrial Flaw Detection, *Atomic Energy Science and Technology, 9* (1961), pp. 455-462
[7] Chen, S.Y., *et al*., 25 MeV Electronic Induction Accelerator for Non-Destructive Testing of Oil Drilling Bits, *Nuclear Techniques, 6* (1984), pp. 35-37 + 66
[8] Chen, S.Y., *et al*., An Electronic Induction Accelerator Made by Tsinghua University, *Atomic Energy Science and Technology, 2* (1960), pp. 87-91
[9] Yu, J. W., Design Method of Electron Induction Accelerator Magnetic Pole, *Atomic Energy Science and Technology, 10* (1961), pp. 552-558
[10] Kerst, D. W., A Process Aiding the Capture of Electrons Injected Into a Betatron, *The Physical Review, 74* (1948), 4, pp. 503-504
[11] Kashkovskii, V. V., Electret Mechanism of Electron Beam Capture by the Magnetic Field of a betatron, *Russian Physics Journal, 49* (2006), 12, pp. 1301-1313
[12] Romanov, V. V., Chakhlov, V. L., Capture of Electrons for Acceleration in a Betatron with Time and Spatial Variation of the Magnetic Field, *Soviet Physics Journal, 31* (1988), 5, pp. 373-376
[13] Wideroe, R., Investigations on the Capturing of Electrons in a 30-MeVBetatron, *Journal of Applied Physics, 22* (1951), 3, pp. 362-363
[14] Adams, G. D., A Method of Increasing Betatron Yield, *The Review of Scientific Instruments, 19* (1948), 401, pp. 607-608
[15] Toprek, D., *et al*., Isochronous Mode of the Future Collector Ring at the Centre for Heavy Ion Research, Darmstadt, Germany, Nuclear technology and radiation protection, 27 (2012), 2, pp: 107-112
[16] Chen, N., *et al*., Research on Numerical Model of Nano-FTIR System Based on COMSOL, *Spectroscopy and Spectral Analysis, 41* (2021), 4, pp. 1125-1130
[17] Cheng, J. E., Accelerator Physics Fundamentals, Peking University Press, Beijing, China, 2012, pp: 102-184
[18] Kolomeytsev, A., *et al.*, Simulation of the Betatron Magnetic Field at the Electron Beam Displacement in Comsol Multiphysics, *MATEC Web of Conferences, 155* (2018), 01039
[19] Zatonov, I., Shtein, M., Numerical Simulation of the Betatron Magnetic Field Using ELCUT Software, *MATEC Web of Conferences, 48* (2016), 03007
[20] Li, X., *et al*., The study of Acceptance and the transmission Efficiency of Separated Sector Cyclotron, *Nucl Technol Radiat, 30* (2015), 1, pp. 18-22
[21] ***, COMSOL Multiphysics, Available at https://cn.comsol.com/multiphysics (accessed on January 1st, 2021)
[22] Zhao, K. H., Chen, X. M., Electromagnetism, Higher Education Press, Beijing, China, 2018, pp. 207-300

Received on February 28, 2022
Accepted on April 27, 2022

Ци ЉУ, Жен-Бо ВАНГ, Ђин-Хај ЛИ, Хај-Тао ВАНГ, Хај-Шенг ЧЕН, Бин ТАНГ

СИМУЛАЦИОНА АНАЛИЗА И ЕКСПЕРИМЕНТ УТИЦАЈА ОБЛИКА МАГНЕТНОГ ПОЛА НА БЕТАТРОН МАГНЕТНО ПОЉЕ

Бетатрони имају предности мале величине, мале тежине и једноставног рада; они се широко користе у испитивању без разарања системима за контролу безбедности терета и возила. Расподела магнетног поља је битан параметар бетатрона и истражена је експерименталним методама. Недавно је симулирана расподела магнетног поља генерисана различитим параметрима магнетних полова. У овој студији коришћена је метода коначних елемената за симулирање расподеле магнетног поља. Симулирани су ефекти на дистрибуцију магнетног поља: различитих углова отварања крајева магнета, величина испупчења полова, броја централних магнетних подлога и ширине дна магнетног пола. На основу резултата симулације пројектован је магнетни пол и мерена је расподела магнетног поља гаусметром. Релативно одступање измерене и симулиране равнотежне орбите је 2.1 %, а релативно одступање индекса распада магнетног поља је 3.3 %. Расподела магнетног поља задовољава битне услове да је магнетно поље на равнотежној орбити бетатрона једнако половини просечног магнетног поља унутар равнотежне орбите, а индекс опадања магнетног поља је већи од нуле и мањи од један. Резултати показују да симулација методом коначних елемената и успостављени модел имају високу поузданост и ефикасно побољшавају тачност пројектовања магнетних полова.

Кључне речи: бетатрон, магнетно поље, магнетни пол, метода коначних елемената